scientific reports



OPEN

Generalized Navier-Stokes model for ballistic and tomographic electrons

Jorge Estrada-Álvarez[™], Francisco Domínguez-Adame & Elena Díaz

Electron hydrodynamics features a plethora of effects where electrons behave like a fluid. Its description relies on hydrodynamic models akin to the Navier-Stokes equations, which progressively lose accuracy when approaching the ballistic regime. In this paper, we derive a generalized Navier-Stokes differential equation with suitable boundary conditions for the drift velocity field in a channel. It still admits a closed-form solution in a uniform channel while spanning the range of validity of hydrodynamic models. It also includes electron tomographic dynamics, a realistic description of electron-electron collisions that affect electrical transport, and explains the occurrence of positive and negative magnetoresistance at low magnetic fields. The model describes phenomena missed by the conventional electron hydrodynamic description, and it generally improves its accuracy.

Electron transport in two-dimensional materials such as graphene¹⁻⁴, gallium arsenide heterostructures⁵, PdCoO₂^{6,7} or Weyl semimetals as WTe₂⁸ results in hydrodynamic signatures resembling conventional fluids⁹⁻¹². Archetypal hydrodynamic signatures are Poiseuille's flow in channels, or the superballistic effect¹³⁻¹⁶, which reduces the resistance of the devices below the ballistic limit. Together with applications for high-frequency operation^{17,18}, the hydrodynamic character of electrons mitigates dissipation while miniaturizing electronic devices^{19,20}. Electron transport in these materials is primarily non-ohmic¹². Therefore, we need the equivalent of Ohm's law to design devices based on two-dimensional materials, especially if they are required to operate in the hydrodynamic regime. Models analogous to the stationary Navier-Stokes equations are often used^{1,2,10,12}, with the electron's drift velocity u(x), or expected value of the velocity, along a uniform channel [see Fig. 1a], satisfies the following equation²¹

$$-\nu \frac{\mathrm{d}^2 u(x)}{\mathrm{d}x^2} + \frac{\mathrm{v}_F}{l_{\mathrm{mr}}} u(x) + \frac{e\mathrm{v}_F E_y}{\hbar k_F} = 0, \tag{1}$$

where ν is the viscosity, dependent on the electronic collision rates and the magnetic field, as we will see later. We use $l_{\rm mr}$ for the mean free path for ohmic collisions against defects and phonons, k_F and ${\bf v}_F$ are the Fermi momenta and Fermi velocity, and $-eE_y$ accounts for a constant force due to the electric potential drop along the channel. In this model, the applied field compensates for the viscous friction associated with a non-uniform velocity of the electron fluid and the ohmic collisions. The velocity profile becomes 22

$$u(x) = \alpha \cosh\left(\sqrt{\frac{\mathbf{v}_F}{\nu l_{\text{mr}}}}x\right) - \frac{e \, l_{\text{mr}} E_y}{\hbar k_F},\tag{2}$$

where α is determined by the edge scattering²³. The advection term $(u \cdot \nabla) u$ of the Navier-Stokes equation, negligible for the low currents attained in common experiments^{3,14}, is strictly zero in a channel geometry where u=(0,u(x)). We consider an incompressible flow for a uniform carrier density, as set by a back-gate potential. The model is also known as Navier-Stokes-Ohm as it features an additional dissipative term, and it is valid in the hydrodynamic regime. However, it abruptly loses its accuracy in small devices operating in the ballistic regime. Indeed, the Navier-Stokes model cannot reproduce common phenomena, not even qualitatively, in this regime. It neither describes the electron tomographic dynamics, a key difference between electrons and conventional fluids that alters its low-temperature electrical properties^{24–29}, especially the superballistic effect 1^{3–15,20,30}. Unless later renormalized 3¹, the Navier-Stokes model is utterly blind to the particularities of electron-electron collisions 2¹ and so, it gives the same results for conventional and tomographic dynamics. In addition, the Navier-Stokes

GISC, Departamento de Física de Materiales, Universidad Complutense, 28040 Madrid, Spain. [⊠]email: jorgestr@ucm.es

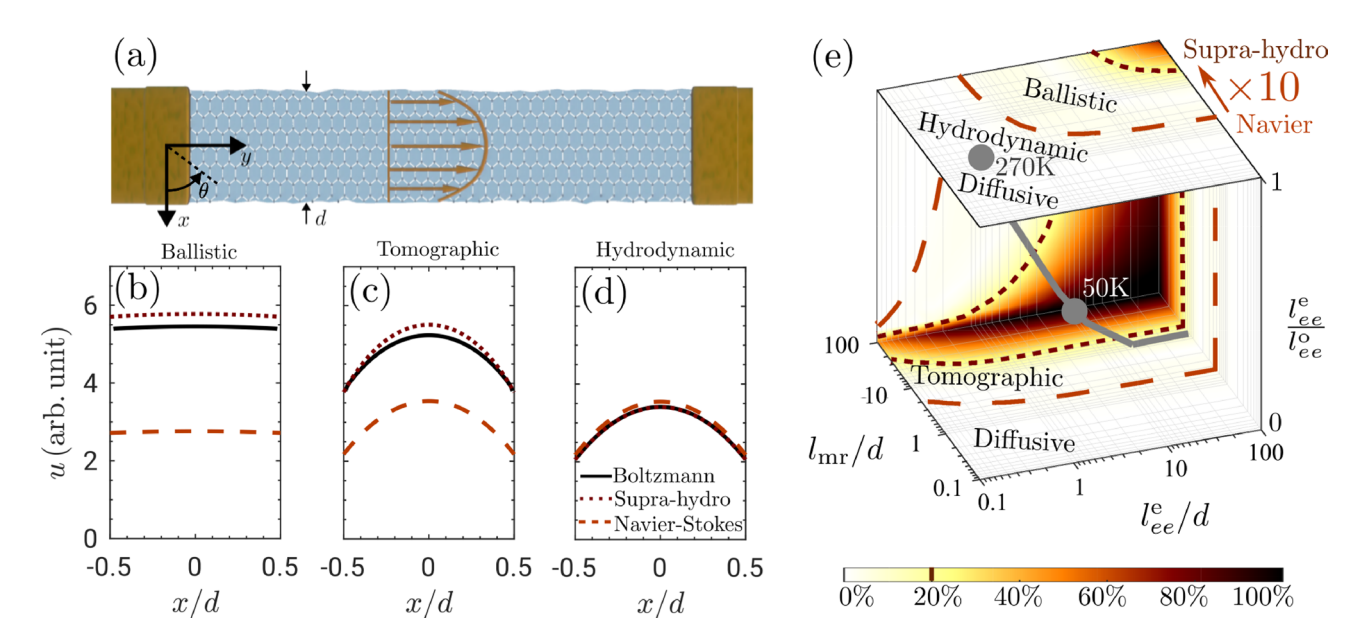


Fig. 1. The supra-hydrodynamic model improves the hydrodynamic model and covers the ballistic and tomographic regimes. (a) Scheme of the considered uniform channel with partially specular edges with $\mathcal{D}=1$ (see "Methods"). Velocity profile in the (b) ballistic $(l_{\rm mr}=l_{ee}^e=l_{ee}^o=20d)$, (c) tomographic $(l_{\rm mr}=10d,l_{ee}^e=0.25d\ll l_{ee}^o)$, and (d) hydrodynamic $(l_{\rm mr}=10d,l_{ee}^e=l_{ee}^o=0.25d)$ regimes. (e) Colormap for the error percentage of the total current evaluated with the supra-hydrodynamic model compared to that simulated with the Boltzmann transport equation. We represent the map as a function of the parameters $l_{\rm mr}/d$, $l_{\rm ee}^{\rm e}/d$ and $l_{\rm ee}^{\rm e}/l_{\rm ee}^{\rm o}$ to consider different transport regimes: diffusive, hydrodynamic and ballistic within classical ($l_{\rm ee}^{\rm o}=l_{\rm ee}^{\rm e}$) and tomographic dynamics ($l_{\rm ee}^{\rm o}\gg l_{\rm ee}^{\rm e}$). Dashed lines limit the regions where the Navier-Stokes error (orange) and the supra-hydrodynamic model (brown) are over a tolerance of 20%. The gray line shows experimental values for a graphene channel 1,14 of width $d=200\,{\rm n}m$ at $n=0.5\times10^{12}\,{\rm cm}^{-2}$. The supra-hydrodynamic model's validity range spans that of Navier-Stokes widely, as indicated by the upper arrow.

model predicts negative magnetoresistance at low fields³², in contrast to many experiments on two-dimensional materials where positive magnetoresistance has been observed^{6,13,33}.

In this work, we propose an extended Navier-Stokes equation, referred to as *supra-hydrodynamic* approach hereafter, consisting of a differential equation for the velocity field to be solved with the appropriate boundary conditions. We analyze the model's range of validity and how it describes the phenomena missed by the Navier-Stokes equation. The supra-hydrodynamic model incorporates realistic electron-electron interactions, accounts for tomographic dynamics, and explains both positive and negative magnetoresistance at low magnetic fields.

Results

Fundamentals

We can study electron viscous flow in two-dimensional materials using the Boltzmann transport equation $^{21,34-37}$. It applies under typical experimental conditions where quantization effects, such as conductance plateaus, are negligible 5,13 . The full distribution f(r,k), such that $f(r,k)/\pi^2$ gives the probability of finding an electron around position r with wavenumber k, obeys

$$\mathbf{v} \cdot \nabla_{\mathbf{r}} f - \frac{e}{\hbar} \left(-\nabla_{\mathbf{r}} V + \mathbf{v} \times \mathbf{B} \right) \cdot \nabla_{\mathbf{k}} f = \Gamma[f], \tag{3}$$

where v and -e are the electron's velocity and charge, respectively. As mentioned before, we consider an isotropic Fermi surface for a constant carrier density n set by a back-gate potential. Electrons are subject to an electric potential V(r) and a perpendicular magnetic field B, with the cyclotron radius $l_b = \hbar k_F/eB$. The collision operator is generally complex³⁸, but in this context it can be simply written as $\Gamma[f] = -v_F \left[(f-f_e) / l_{\rm mr} + (f-f_{ee}) / l_{ee} \right]$. It describes the collisions against defects and phonons, with a mean free path $l_{\rm mr}$, that relax the distribution towards the Fermi distribution f^e . It also takes into account the electron-electron scattering, that relax the distribution towards a Fermi distribution shifted by the electron's mean wavenumber f_{ee} , with a mean free path l_{ee} , that will be distinct for different modes to describe tomographic dynamics^{39,40}, see below. We consider a channel parallel to the y axis of width d and long enough to neglect the region near the contacts, where the electrons experience a potential $-yE_y+V_H(x)$, for a constant field across the channel E_y and where $V_H(x)$ is the Hall potential. We write $\mathbf{k}=(k\cos\theta,k\sin\theta)$ and define the distribution $g(x,\theta)=\int_0^\infty (f-f_e)\,\mathrm{d}k/k_F$ and $g_{ee}(x,\theta)=\int_0^\infty (f_{ee}-f_e)\,\mathrm{d}k/k_F$. Upon integration, we find the differential equation that gives the excess of electrons at position x moving in the direction defined by $\theta^{18,21}$

$$\cos\theta \frac{\partial g}{\partial x} - \frac{e\cos\theta}{\hbar k_F} \frac{\mathrm{d}V_H}{\mathrm{d}x} + \frac{eE_y\sin\theta}{\hbar k_F} + \frac{1}{l_b} \frac{\partial g}{\partial \theta} = \Gamma[g]. \tag{4}$$

Thus, the electron's drift velocity along the channel can be obtained from the distribution as follows 18,21

$$u(x) = \frac{1}{\pi} \int_0^{2\pi} \sin\theta \, g(x, \theta) \, d\theta \tag{5}$$

and, upon integration of u(x) over the spatial coordinate x across the channel, the electrical current is evaluated. Under this formalism, the electron-electron collisions, responsible for the viscous effects, relax the distribution g towards $g_{ee} = u \sin \theta$. The formal study of electron dynamics reveals different rates for each mode in the polar expansion of $g^{25,26}$. Here we will focus on the lower-order modes, which pose the foremost contribution to the electrical properties⁴¹. Indeed, we cast the collision operator as

$$\Gamma[g] = -\frac{g}{l_{\rm mr}} - \frac{g^{\rm e} - g_{ee}^{\rm e}}{l_{ee}^{\rm e}} - \frac{g^{\rm o} - g_{ee}^{\rm o}}{l_{ee}^{\rm o}},\tag{6}$$

where we split $g=g^e+g^o$ into the even and odd modes. The even modes relax with a characteristic l_{ee}^e , while the odd modes relax with an l_{ee}^o . We take an l_{ee}^o representative of the third mode, as higher order odd modes have a smaller contribution to electrical transport. The rates are similar $l_{ee}^e \simeq l_{ee}^o$ at high temperatures, but $l_{ee}^e \ll l_{ee}^o$ when the temperature is much lower than the Fermi temperature, giving rise to tomographic dynamics 39,40 . The Boltzmann equation accurately predicts the transport phenomena in the ballistic, tomographic, and hydrodynamic regimes. However, its complexity makes it impossible to solve it analytically, and numerical simulations are necessary even to address the channel geometry. Remarkably, our formulation of a suprahydrodynamic model enables us to obtain an analytical solution in such cases.

Supra-hydrodynamic model

To derive the supra-hydrodynamic model, we first write $g(x,\theta)$ as a Fourier series up to the fourth-order as follows

$$g(x,\theta) \simeq \sum_{n=1}^{4} \left[s_n(x) \sin n\theta + c_n(x) \cos n\theta \right],$$
 (7)

where $s_1(x)=u(x)$ is the drift velocity according to Eq. (5). The existence of electron-electron collisions guarantees the relaxation of high-order modes and justifies a second-order expansion²¹. Therefore, the suprahydrodynamic model generalizes it, providing a wider range of validity that we will analyze. Equation (7) is substituted into the Boltzmann equation to set a system of equations. In the absence of the magnetic field, $c_n=0$, which allows us to write a system of four coupled linear differential equations for u, s_2 , s_3 , and s_4 , and after some algebra, s_2 , s_3 , and s_4 coefficients can be eliminated (see "Methods"). The supra-hydrodynamic equation finally reads

$$\left(\eta \frac{\mathrm{d}^4}{\mathrm{d}x^4} - \nu \frac{\mathrm{d}^2}{\mathrm{d}x^2} + \frac{\mathrm{v}_F}{l_{\mathrm{mr}}}\right) u(x) + \frac{e\mathrm{v}_F E_y}{\hbar k_F} = 0,\tag{8}$$

which generalizes the Navier-Stokes model with the following modified viscosity

$$\nu = \frac{3\gamma_{\rm mr} + 2\gamma_{\rm o}}{8\gamma_{\rm o}\gamma_{\rm o}} \, v_F \tag{9}$$

and a new term dependent on the fourth derivative of the velocity multiplied by

$$\eta = \frac{1}{32\gamma_o^2\gamma_o} \mathbf{v}_F. \tag{10}$$

For the sake of brevity, we have defined the following rates related to electronic collisions: $\gamma_{\rm mr}=1/l_{\rm mr}$, $\gamma_{\rm e}=1/l_{\rm mr}+1/l_{ee}^{\rm e}$ and $\gamma_{\rm o}=1/l_{\rm mr}+1/l_{ee}^{\rm o}$.

As well as the Navier-Stokes model, Eq. (8) is a linear differential equation that admits a closed-form solution in the channel depicted in Fig. 1a

$$u(x) = \alpha_1 \cosh(\lambda_1 x) + \alpha_2 \cosh(\lambda_2 x) - \frac{e l_{\text{mr}} E_y}{\hbar k_F}, \tag{11}$$

where

$$\lambda_1 = \sqrt{\frac{\nu}{2\eta} \left[1 + \sqrt{1 - \frac{4v_F \eta \gamma_{\text{mr}}}{\nu^2}} \right]} \qquad \lambda_2 = \sqrt{\frac{\nu}{2\eta} \left[1 - \sqrt{1 - \frac{4v_F \eta \gamma_{\text{mr}}}{\nu^2}} \right]}. \tag{12}$$

Moreover, α_1 and α_2 are analytically determined upon imposing boundary conditions at the edges (see "Methods")²³. Last, the velocity profile (11) can be easily integrated over the coordinate x to obtain the total current and the resistance.

Figure 1b shows a ballistic velocity profile for $l_{\rm mr}=l_{ee}^e=l_{ee}^o=20d$ and a partially specular edge. In such a case, the Navier-Stokes model fails, while the supra-hydrodynamic one reproduces accurately the profile given by the Boltzmann equation. The latter also successfully explains the deep tomographic regime and the curvature of the profile in Fig. 1c for $l_{\rm mr}=10d$, $l_{ee}^e=0.25d\ll l_{ee}^o$, that the standard hydrodynamic model cannot account for. Unlike the Navier-Stokes equation, which is blind to the peculiarities of the tomographic dynamics, the supra-hydrodynamic coefficients of Eq. (8), ν and η , distinguish the relaxation rates of the even ($\gamma_{\rm e}$) and odd parity ($\gamma_{\rm o}$) modes. Indeed, it accounts for the velocity profiles and explains the lower resistance under tomographic collisions, which do not relax the odd parity modes of the distribution function. The generalized model also predicts the profile and the so-called slip-length, which characterizes the edge scattering, similar to previous descriptions 42,43, not shown for brevity. Figure 1d shows a case where the regime of transport is hydrodynamic ($l_{\rm mr}=10d$, $l_{\rm ee}^e=l_{\rm ee}^o=0.25d$) and therefore, both Navier-Stokes and the proposed suprahydrodynamic model agree with Boltzmann equation prediction.

Figure 1e shows the accuracy of the supra-hydrodynamic model²¹. In these simulations, we consider a uniform channel with rough edges for a better comparison, although the general conclusion is also valid for specular edges that would produce lower errors²¹. Figure 1e demonstrates that, although the model is not valid in the ultra-deep ballistic regime $l_{\rm mr}$, $l_{ee} \to \infty$, it leads to successful results under typical experimental conditions where the ballistic regime is usually studied^{1-3,14,33}. It is demonstrated that the supra-hydrodynamic model properly describes the transport and electrical properties under the diffusive, hydrodynamic, ballistic and tomographic regimes.

Supra-hydrodynamic model with a magnetic field

Now, let us consider the effects of a perpendicular magnetic field in our generalized model. An algebraic derivation similar to that of the previous section yields the following supra-hydrodynamic equation

$$\left(-\chi \frac{\mathrm{d}^6}{\mathrm{d}x^6} + \eta \frac{\mathrm{d}^4}{\mathrm{d}x^4} - \nu \frac{\mathrm{d}^2}{\mathrm{d}x^2} + \frac{\mathrm{v}_F}{l_{\mathrm{mr}}}\right) u(x) + \frac{\mathrm{e}\mathrm{v}_F E_y}{\hbar k_F} = 0,$$
(13)

where the viscosity is replaced by

$$\nu = \frac{v_F}{4 (\gamma_e^2 + 4 \gamma_b^2)} \left[\gamma_e + 3 \gamma_{mr} \frac{\gamma_o (\gamma_e^3 + 12 \gamma_e \gamma_b^2) - (8 \gamma_e^2 \gamma_b^2 + 80 \gamma_b^4)}{(\gamma_o^2 + 9 \gamma_b^2) (\gamma_e^2 + 16 \gamma_b^2)} \right]$$
(14)

with $\gamma_b = 1/l_b$. Here, the first term accounts for the dependence of the viscosity on the magnetic field in the Navier-Stokes model²¹. We also introduce the coefficients

$$\eta = \frac{v_F \left[\gamma_e^2 \left(9 \gamma_{mr} + 8 \gamma_o \right) + 4 \gamma_b^2 \left(25 \gamma_{mr} - 12 \gamma_e + 16 \gamma_o \right) \right]}{64 \left(\gamma_e^2 + 4 \gamma_b^2 \right) \left(\gamma_o^2 + 9 \gamma_b^2 \right) \left(\gamma_e^2 + 16 \gamma_b^2 \right)},$$
(15)

$$\chi = \frac{3 \,\mathrm{v}_F \,\gamma_{\rm e}}{256 \left(\gamma_{\rm e}^2 + 4\gamma_b^2\right) \left(\gamma_{\rm o}^2 + 9\gamma_b^2\right) \left(\gamma_{\rm e}^2 + 16\gamma_b^2\right)}.$$
 (16)

Similar to Eq. (11), the solution in a uniform channel in the presence of a magnetic field now reads

$$u(x) = \sum_{n=1}^{3} \alpha_n \cosh(\lambda_n x) - \frac{e \ l_{\text{mr}} E_y}{\hbar k_F},\tag{17}$$

where $\lambda_n = \sqrt{\Lambda_n}$ are obtained after solving the cubic equation $-\chi \Lambda^3 + \eta \Lambda^2 - \nu \Lambda + \gamma_{\rm mr} = 0$, and the boundary condition²³ establishes α_1 , α_2 , and α_3 .

Figures 2a–c show the velocity profiles of a uniform channel with partially specular boundaries in a ballistic regime of transport, $l_{\rm mr}=5d$, l_{ee}^e and $l_{ee}^o\gg d$, when a magnetic field is applied. Fields are expressed in units of the commensurability field $B_c=\hbar k_F/ed^{44}$ such that (a) B=0, (b) $B=0.5B_C$ and (c) $B=B_C$. Note that the boundary conditions (see "Methods") are derived under the hypothesis that the distribution g at the edges is a smooth function. However, this is not the case near the commensurability condition $B=B_C$ so this inaccuracy will affect the results shown in Fig. 2c. A more accurate description could be obtained using numerical calculations to obtain a boundary condition under a magnetic field 45,46 , but the goal of this article is to obtain a simple closed-form model, so we keep this level of approximation with valid results. Indeed, as shown in Fig. 2a and b, the supra-hydrodynamic model already works properly under a magnetic field, away from the commensurability condition $B\sim B_c$, and it improves the predictions of the standard Navier-Stokes model.

Most remarkably, the supra-hydrodynamic model reproduces the positive magnetoresistance observed at low fields in experiments performed beyond the fully hydrodynamic transport³² [see Fig. 2d] and provides an accurate description in the deep tomographic regime [see Fig. 2e]. On the contrary, the Navier-Stokes model misses this effect, and it always predicts negative magnetoresistance [see Fig. 2d–f].

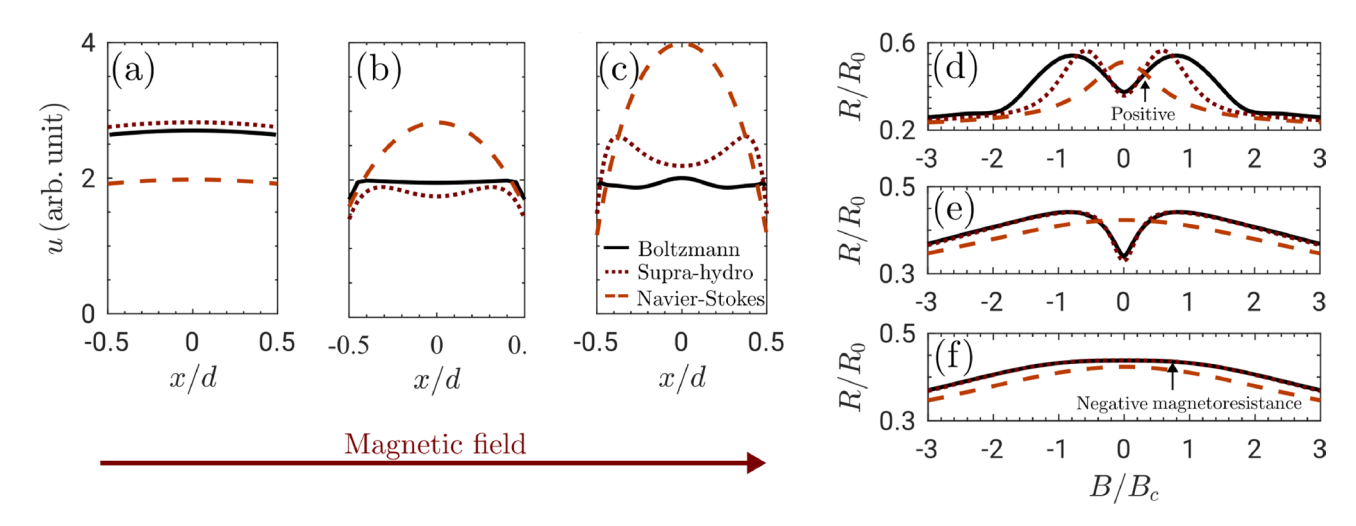


Fig. 2. The supra-hydrodynamic model improves the results of the Navier-Stokes equation under a magnetic field. Velocity profile of a uniform channel with specular edges ($\mathcal{D}=1$, see "Methods") in a ballistic regime of transport with $l_{\rm mr}=5d$, l_{ee}^e and $l_{ee}^o\gg d$ in the presence of a magnetic field: (a) B=0, (b) $B=0.5B_c$, and (c) $B=B_c$, where $B_c=\hbar k_F/ed$ is the commensurability magnetic field. Magnetoresistance curves for different regimes of transport and $d/l_{mr}=0.2$: (d) Ballistic with $d/l_{ee}^e=d/l_{ee}^o=0$, (e) deep tomographic with $d/l_{ee}^e=4$ but $d/l_{ee}^o=0$, and (f) fully hydrodynamic with $d/l_{ee}^e=d/l_{ee}^o=4$.

Discussion

The inherent complexity of the Boltzmann equation is often circumvented by employing simpler hydrodynamic models, such as those based on the Navier-Stokes equation. However, they miss relevant phenomena, from the tomographic dynamics of electrons^{25,27} to the occurrence of positive magnetoresistance³³. Just as the Burnett equations generalized the Navier-Stokes equations in a conventional fluid⁴⁷, our supra-hydrodynamic model generalizes the hydrodynamic models for electrons, with potential interest for other particle systems as phonons⁴⁸. In electronic systems transport phenomena usually occur near the Fermi surface, and we can exploit that fact to write the electron distribution as a Fourier expansion in the polar angle. Despite the drastic differences in the derivation and the final equations of our model, adding higher order terms to the Navier-Stokes, similar to the Chapman-Enskog expansion⁴⁹, has shown its usefulness in the description of conventional fluids⁵⁰. Nevertheless, the Burnett equations have mathematical pathologies and convergence issues, which have been studied in detail^{51,52}. On the contrary, our model is more closely related to the better-behaved harmonic expansion in semiconductors⁵³, where hydrodynamic expansions have been used⁵⁴. Therefore, it reveals the appropriate generalized model for electron hydrodynamics.

Moreover, key phenomena of electron fluids, such as tomographic dynamics or the correct sign in the magnetoresistance, are missed by the Navier-Stokes equation. Together with the experimental difficulty to fully achieve the hydrodynamic regime, $l_{ee} \ll d$, other attempts to dodge the Boltzmann equation have been made using non-local conductivity tensors where the description of all polar modes is included^{25,39,40,55}. The suprahydrodynamic model enables analytic solutions to describe the variety of edge-scattering mechanisms usually found in experiments^{2,3,23}. It is to be noticed that expansions of the Boltzmann equation to second order may also describe boundary layers accurately^{42,43,56}. Another remarkable expansion of the Boltzmann equation up to third-order was addressed in the quasi-hydrodynamic by Alekseev and Dimitriev for the description of magnetotransport⁵⁷. However, our expansion to the fourth order is even more accurate, and replacing the Boltzmann equation with a supra-hydrodynamic model, where we write the equations and boundary conditions just in terms of the velocity field, facilitates a more straightforward interpretation of the results.

Conclusion

In this work, we introduce a generalized Navier-Stokes equation that extends the range of validity of conventional electron hydrodynamic models by one order of magnitude. Remarkably, our approach properly describes hydrodynamic, tomographic, and ballistic electrons under typical experimental conditions. This formulation incorporates appropriate boundary conditions and retains analytical solutions in uniform geometries, facilitating its application. In particular, the supra-hydrodynamic model correctly predicts the positive or negative sign of the magnetoresistance in two-dimensional materials at low magnetic fields, overcoming the limitations of conventional hydrodynamic approaches. The introduced framework provides a more accurate and comprehensive description of the collective behavior of electrons, especially in the transition toward ballistic transport.

Methods Model derivation

We can derive the supra-hydrodynamic model by writing the $g(x,\theta)$ as the fourth-order Fourier expansion in Eq. (7). We use fundamental relationships to expand the product of trigonometric functions as a sum, and we write the collision operator as

$$\Gamma[g] = \gamma_{\rm mr} u \sin \theta + \gamma_{\rm mr} c_1 \cos \theta + \gamma_e s_2 \sin 2\theta + \gamma_e c_2 \cos 2\theta + \gamma_o s_3 \sin 3\theta + \gamma_o c_3 \cos 3\theta + \gamma_e s_4 \sin 4\theta + \gamma_e c_4 \cos 4\theta, \quad (18)$$

where $u=s_1$ is the electron's drift velocity. We show that $c_1=0$ as there is no net current through the edge of the channel²³. We substitute the expansion in Eq. (4), group the resulting terms with each trigonometric function, and impose each as zero. Note that the terms with sine and cosine functions are decoupled without a magnetic field. The condition $c_2=c_3=c_4=0$ follows from $c_1=0$, while the remaining equations read

$$\gamma_{\text{mr}} u + \frac{1}{2} \frac{ds_2}{dx} = -\frac{eE_y}{\hbar k_F},$$

$$\gamma_e s_2 + \frac{1}{2} \frac{du}{dx} + \frac{1}{2} \frac{ds_3}{dx} = 0,$$

$$\gamma_o s_3 + \frac{1}{2} \frac{ds_2}{dx} + \frac{\beta}{2} \frac{ds_4}{dx} = 0,$$

$$\gamma_e s_4 + \frac{1}{2} \frac{ds_3}{dx} = 0.$$
(19)

The fourth-order Fourier expansion is just an approximation to the full solution of the Boltzmann equation, which, ideally, has infinite terms. Substituting it directly gives this set of equations with $\beta=1$ and an additional condition $\mathrm{d}s_4/\mathrm{d}x=0$, which cannot be fulfilled together with these equations. Therefore, in a finite expansion up to fourth order, we might ignore the additional condition $\mathrm{d}s_4/\mathrm{d}x=0$. But $\mathrm{d}s_4/\mathrm{d}x$ also appears in the third equation. So, rather than ignoring it, we can take $\beta=1/2$ in Eq. (19), which slightly improves the accuracy of using $\beta=1$. We derive the expressions in Eq. (19) three times with respect to x and obtain a linear coupled system of equations. In this system, we perform Gaussian elimination to isolate s_2 , s_3 , and s_4 , obtaining an equation only for u and its derivatives. A typical process in ordinary differential equations is to reduce the order of an equation for u and its higher order derivatives by adding new variables, such as defining new magnitudes like $\mathrm{d}u/\mathrm{d}x$ or $\mathrm{d}^2u/\mathrm{d}x^2$ for the high order derivatives. Here, we follow the opposite process: We eliminate the superfluous variables by increasing the order of the equation and obtain the result given by Eq. (8). We can expand g to different orders, writing extended versions of (19), whose results are depicted in Fig. 3. The M=4 model discussed in the paper strikes a balance between the complexity of the expressions and the accuracy of the results.

We can follow an analog procedure in the presence of a magnetic field to obtain the following set of coupled equations

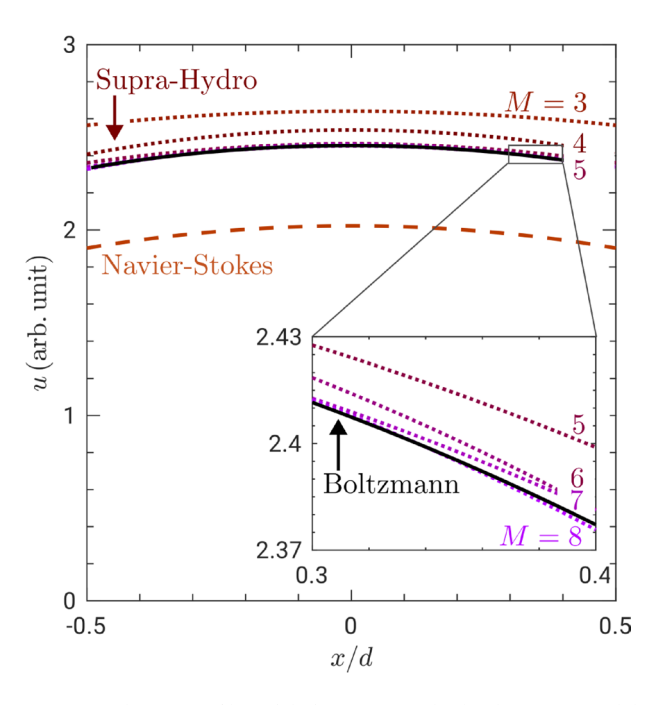


Fig. 3. Velocity profiles of different supra-hydrodynamic models. The order M=4 corresponds to the supra-hydrodynamic model explored in this article. Increasing M results in a better convergence to the result of the Boltzmann equation. We consider $l_{\rm mr}=l_{ee}^e=l_{ee}^o=5d$ and a partially specular $\mathcal{D}=1$ edge.

$$\frac{1}{2} \frac{dc_1}{dx} = 0,$$

$$\gamma_{\text{mr}} c_1 + \gamma_b u + \frac{1}{2} \frac{dc_2}{dx} = \frac{e}{\hbar k_F} \frac{dV_H}{dx},$$

$$-\gamma_b c_1 + \gamma_{\text{mr}} u + \frac{1}{2} \frac{ds_2}{dx} = -\frac{eE_y}{\hbar k_F},$$

$$\gamma_e c_2 + 2\gamma_b s_2 + \frac{1}{2} \frac{dc_1}{dx} + \frac{1}{2} \frac{dc_3}{dx} = 0,$$

$$-2\gamma_b c_2 + \gamma_e s_2 + \frac{1}{2} \frac{du}{dx} + \frac{1}{2} \frac{ds_3}{dx} = 0,$$

$$\gamma_o c_3 + 3\gamma_b s_3 + \frac{1}{2} \frac{dc_2}{dx} + \frac{\beta}{2} \frac{dc_4}{dx} = 0,$$

$$-3\gamma_b c_3 + \gamma_o s_3 + \frac{1}{2} \frac{ds_2}{dx} + \frac{\beta}{2} \frac{ds_4}{dx} = 0,$$

$$\gamma_e c_4 + 4\gamma_b s_4 + \frac{1}{2} \frac{dc_3}{dx} = 0,$$

$$-4\gamma_b c_4 + \gamma_e s_4 + \frac{1}{2} \frac{ds_3}{dx} = 0.$$
(20)

We again take derivatives three times and use Gaussian elimination to obtain two equations for u, V_H , and their derivatives. Additionally, if we focus on the velocity field, we can derive these expressions twice and find an equation only for the velocity field, which is Eq. (13).

Boundary conditions

Edge scattering determines the electrical properties in the hydrodynamic, tomographic, and ballistic regimes²³. By considering the appropriate boundary conditions in the supra-hydrodynamic model, we can describe particular edge scattering properties, either by a rough or a partially specular edge.

We can derive boundary conditions by writing the distribution at the x = d/2 edge

$$g(\theta) = \tilde{u}\sin\theta + \tilde{s}_2\sin 2\theta, \tag{21}$$

where $-\pi/2 < \theta < \pi/2$ account for the incident electrons. The parameterization of g as a function of \tilde{u} and \tilde{s}_2 , which is exact in the hydrodynamic fluid-like regime²¹, still provides reasonable results in the tomographic and ballistic regimes, as evidenced by the range of validity of the supra-hydrodynamic model. A phenomenological approach to typical edge scattering considers a very rough, disordered edge that scatters the electrons in all directions^{2,3,23}. The scattered distribution in this case is

$$g^{(R)}(\theta) = 0, (22)$$

where $\pi/2 < \theta < 3\pi/2$ are the angles of the scattered electrons. After combining Eqs. (21) and (22), we obtain the following expansion

$$g(\theta) \simeq u \sin \theta + s_2 \sin 2\theta + s_3 \sin 3\theta + s_4 \sin 4\theta \tag{23}$$

with the Fourier coefficients

$$\begin{pmatrix} u \\ s_2 \\ s_3 \\ s_4 \end{pmatrix} = \begin{pmatrix} 1/2 & 4/3\pi \\ 4/3\pi & 1/2 \\ 0 & 4/5\pi \\ -8/15\pi & 0 \end{pmatrix} \begin{pmatrix} \tilde{u} \\ \tilde{s}_2 \end{pmatrix}. \tag{24}$$

After some algebra it is possible to eliminate \tilde{u} and \tilde{s}_2 by imposing

$$A (u s_2 s_3 s_4)^T = 0, (25)$$

so that edge scattering constrains the shape of the distribution function at the edges. Particularly for a rough (R) edge, the matrix reads

$$A^{(R)} = \begin{pmatrix} 1.55 & -1.82 & 1 & 0 \\ 1.21 & -1.03 & 0 & 1 \end{pmatrix}. \tag{26}$$

Another approach to edge scattering is a partially specular edge (S) with a scattered distribution 13,23

$$g^{(S)}(\theta) = g(\pi - \theta) + \mathcal{D}\cos\theta \times \left[g(\pi - \theta) - \frac{2}{\pi} \int_{\pi/2}^{3\pi/2} \cos^2\theta' g(\pi - \theta') d\theta'\right]$$
(27)

for $\pi/2 < \theta < 3\pi/2$ and the incident distribution given by Eq. (21). The dispersion coefficient $\mathcal{D} = \sqrt{\pi} h^2 h' k_F^3 \lesssim 1$ is related to the edge's bumps height h and its correlation length h'^{23} . Edge scattering can also be modeled in great detail using the Berry-Mondragon condition, which also results in partial scattering of the electrons and has been used to calculate the electrical properties of nanoribbons^{58,59}. For a partially specular edge, the matrix of Eq. (25) reads

$$A^{(S)} = \begin{pmatrix} \frac{0.151 \, \mathcal{D} - 1}{0.075 \, \mathcal{D} - 1} & -\frac{0.167 \, \mathcal{D}^2 - 1.963 \, \mathcal{D} + 4}{\mathcal{D} - 0.075 \, \mathcal{D}^2} & 1 & 0\\ -\frac{0.19 \, \mathcal{D}}{0.075 \, \mathcal{D} - 1} & -\frac{0.162 \, \mathcal{D} - 0.762}{0.075 \, \mathcal{D} - 1} & 0 & 1 \end{pmatrix}. \tag{28}$$

In order to write the boundary conditions for the velocity field u, we carry out Gaussian elimination in the linear system defined by Eq. (19) and its derivatives to write each of the s_2 , s_3 , and s_4 as a function of the velocity field and its derivatives as follows

$$(u s_2 s_3 s_4)^T = B (u u^{(1)} u^{(2)} u^{(3)})^T + B_0,$$
(29)

where the conversion matrices are

$$B = \begin{pmatrix} 1 & 0 & 0 & 0\\ 0 & -\frac{3\gamma_{\rm mr} + 2\gamma_{\rm o}}{4\gamma_{\rm e}\gamma_{\rm o}} & 0 & \frac{1}{16\gamma_{\rm e}^2\gamma_{\rm o}}\\ \frac{3\gamma_{\rm mr}}{2\gamma_{\rm o}} & 0 & -\frac{1}{8\gamma_{\rm e}\gamma_{\rm o}} & 0\\ 0 & -\frac{3\gamma_{\rm mr}}{4\gamma_{\rm e}\gamma_{\rm o}} & 0 & \frac{1}{16\gamma_{\rm e}^2\gamma_{\rm o}} \end{pmatrix}$$
(30)

and

$$B_0 = \left(0 \ 0 \ \frac{-3}{2 \gamma_0} \ 0\right)^T. \tag{31}$$

Now we impose two equations for the velocity field and its derivatives at the boundary such that

$$AB\left(u\ u^{(1)}\ u^{(2)}\ u^{(3)}\right)^{T} = -AB_{0},$$
 (32)

where these matrices replace the slip-length ξ in the hydrodynamic boundary condition $u=-\xi u^{(1)}$, improving its accuracy. In particular, in a channel, we define two additional matrices C and C_0 as follows

$$C = \begin{pmatrix} \cosh\left(\frac{\lambda_1 d}{2}\right) & \cosh\left(\frac{\lambda_2 d}{2}\right) \\ \lambda_1 \sinh\left(\frac{\lambda_1 d}{2}\right) & \lambda_2 \sinh\left(\frac{\lambda_2 d}{2}\right) \\ \lambda_1^2 \cosh\left(\frac{\lambda_1 d}{2}\right) & \lambda_2^2 \cosh\left(\frac{\lambda_2 d}{2}\right) \\ \lambda_1^3 \sinh\left(\frac{\lambda_1 d}{2}\right) & \lambda_2^3 \sinh\left(\frac{\lambda_2 d}{2}\right) \end{pmatrix}, \tag{33}$$

$$C_0 = \left(\frac{-e\mathbf{v}_F l_{\mathrm{mr}} E_y}{\hbar k_F \mathbf{v}_F} \ 0 \ 0 \ 0\right)^T,\tag{34}$$

and substitute the closed-form solution of Eq. (11) to obtain the following 2×2 linear system that gives c_1 and c_2

$$ABC\begin{pmatrix} \alpha_1 \\ \alpha_2 \end{pmatrix} = -AB_0 - ABC_0. \tag{35}$$

The generalization of the boundary conditions in the presence of a magnetic field is possible by writing the distribution for the incident electrons at x=d/2 as a Fourier series with up to second-order

$$g(\theta) = \tilde{c}_0 + \tilde{u}\sin\theta + \tilde{c}_1\cos\theta + \tilde{s}_2\sin2\theta + \tilde{c}_2\cos2\theta, \tag{36}$$

where $-\pi/2 < \theta < \pi/2$ and now the \tilde{c}_n coefficients may not be zero in a magnetic field. We supplement it with the no-trespassing condition²³, accounting for charge conservation at the boundary. Similarly, this expression, which enables the determination of a boundary condition without premises on the device geometry, is exact in the hydrodynamic regime and is a general way to derive a boundary condition without assuming any particular geometry. However, it is not valid near the commensurability condition $d \sim l_b$ ($B \sim B_C$), where the electrons arriving from the other edge of the channel alter the distribution. Even for the conventional hydrodynamic model, which characterizes edge scattering with a simple slip-length ξ , a more detailed characterization of edge scattering requires numerical calculations^{45,46}. In a similar way as in the absence of magnetic field, we use the distributions for the scattered electrons in Eqs. (22) and (27), write g as a Fourier sum, and find the A matrix with three equations for $u, s_2, s_3, s_4, c_2, c_3, c_4$. We derive B upon Gaussian elimination in Eq. (20) and its derivatives, writing each of these variables in terms of $u, \ldots, u^{(5)}$. To facilitate its implementation, we provide the resulting matrix in the Supplementary Material. In particular, in a channel geometry, we can write a 3×3 linear system

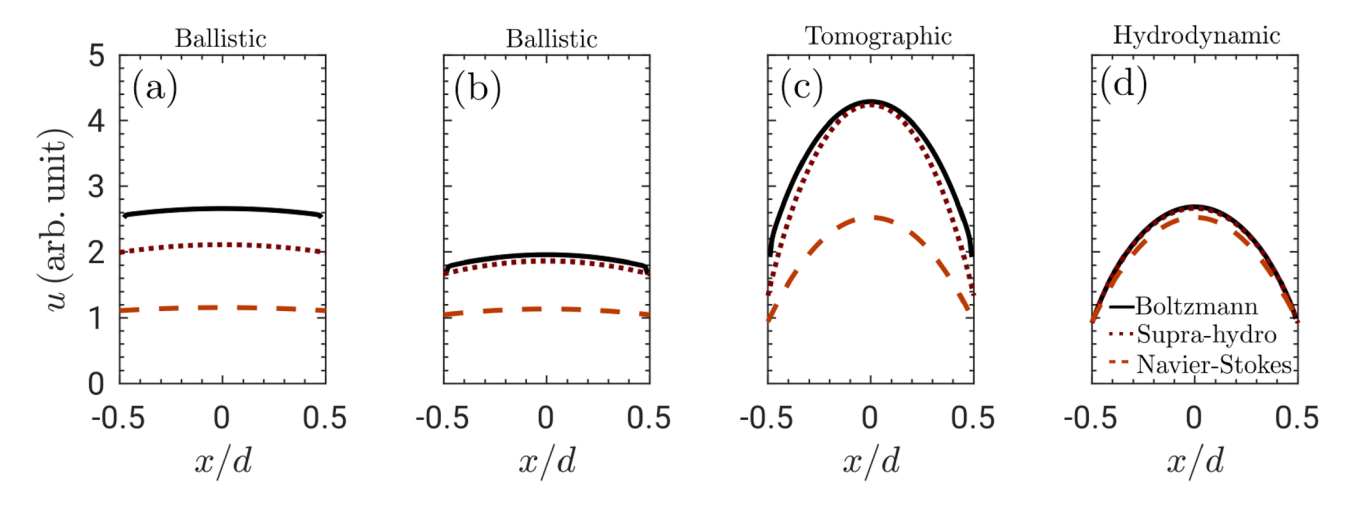


Fig. 4. Velocity profiles for a rough edge. (a) Ballistic regime ($l_{\rm mr}=l_{ee}^{\rm e}=l_{ee}^{\rm o}=20d$), to be compared with the partially specular edge in Fig. 1(b). (b) Ballistic regime ($l_{\rm mr}=l_{ee}^{\rm e}=l_{ee}^{\rm o}=10d$). (c) Tomographic regime ($l_{\rm mr}=10d, l_{ee}^{\rm e}=0.25d \ll l_{ee}^{\rm o}$), to be compared with Fig. 1(c). (d) Hydrodynamic regime ($l_{\rm mr}=10d, l_{ee}^{\rm e}=l_{ee}^{\rm o}=0.25d$), to be compared with Fig. 1(d).

$$ABC \begin{pmatrix} \alpha_1 \\ \alpha_2 \\ \alpha_3 \end{pmatrix} = -AB_0 - ABC_0, \tag{37}$$

which we solve for α_1 , α_2 and α_3 , the coefficients that determine the current profile. In the manuscript, we primarily present results for a partially specular edge. Figure 4 also illustrates their analogue for a rough edge, where convergence, slightly slower, is still achieved in the ballistic regime.

Numerical methods

We compare the closed-form solution provided by the supra-hydrodynamic model against the Boltzmann equation, which must be solved numerically²¹. We use a conforming Galerkin finite element method^{21,60}, approximating the distribution function as follows

$$g(x,\theta) = \sum_{n=1}^{N} \sum_{m=1}^{M} g_{nm} \,\phi_n(x) \,\varphi_m(\theta), \tag{38}$$

where $\{\phi_n(x)\}$ is a basis of tent functions defined on the [-d/2,d/2] interval and the products of adjacent tent functions, and $\{\varphi_m(\theta)\}$ is a set of periodic tent function defined for $[0,2\pi)$. We achieve convergence with $\mathcal{N}=60$ and $\mathcal{M}=32$. We impose centered Fermi surfaces and the boundary condition for reflected electrons at the edges. We write the weak formulation of the Boltzmann equation and solve the subsequent linear system for the g_{nm} coefficients. We numerically integrate the distribution to give the drift velocity u. The integration of the velocity profile gives the total current $I \propto \int_{-d/2}^{d/2} u(x) \, \mathrm{d}x$ and the resistance. We evaluate the relative error of the supra-hydrodynamic (SH) model in comparison with the Boltzmann equation (BTE) results as $|I_{\mathrm{SH}}-I_{\mathrm{BTE}}|/I_{\mathrm{BTE}}$.

Navier-Stokes model

In previous sections, we have also shown the profiles obtained with the conventional Navier-Stokes model. We can also obtain it from the Boltzmann equation upon the hypothesis of collective fluid-like behavior²¹

$$g(x,\theta) \simeq \sum_{n=1}^{2} \left[s_n(x) \sin n\theta + c_n(x) \cos n\theta \right]. \tag{39}$$

The supra-hydrodynamic model relaxes this condition by adding the contribution of higher-order modes in the Fourier expansion, extending its range of validity. Upon the assumption of Eq. (39), the Boltzmann equation reduces to the Navier-Stokes equation in a channel as

$$-\nu \frac{d^2 u(x)}{dx^2} + \frac{v_F}{l_{\text{mr}}} u(x) + \frac{e v_F E_y}{\hbar k_F} = 0,$$
(40)

where $\nu = v_F \gamma_e/(4\gamma_e^2 + 16\gamma_b^2)$ is the viscosity. Edge scattering is characterized with an slip-length ξ^{23} imposing the boundary condition $u(x) = -\xi du(x)/dx$. In particular, $\xi = 2.35 \, \nu/v_F$ for the rough edge and

 $\xi=(8/\mathcal{D}-1.70)\nu/v_F$ for the partially specular one. The velocity profile, defining $\lambda=\sqrt{v_F/\nu l_{\rm mr}}$, is written as

$$u(x) = -\frac{ev_F l_{\rm mr} E_y}{\hbar k_F v_F} \left[1 - \frac{\cosh \lambda x}{\cosh(\lambda d/2) + \xi \lambda \sinh(\lambda d/2)} \right]. \tag{41}$$

Particularly, in the limit of no collisions against impurities $l_{\rm mr} \to \infty$ and under frequent electron-electron collisions $l_{ee} \ll d$, which ensures $\xi/d \ll 1$, we find a parabolic profile of the conventional Poiseuille flow:

$$u(x) \simeq -\frac{e\mathbf{v}_F E_y}{2\hbar k_F \nu} \left[\left(\frac{d}{2} \right)^2 - x^2 \right]. \tag{42}$$

In this work, Eqs. (11) and (17) provide more accurate expressions for the velocity profile under the suprahydrodynamic model.

Data availability

The datasets used and/or analysed during the current study available from the corresponding author on reasonable request.

Received: 13 March 2025; Accepted: 26 September 2025

Published online: 03 November 2025

References

- 1. Bandurin, D. et al. Negative local resistance caused by viscous electron backflow in graphene. Science 351, 1055-1058 (2016).
- 2. Palm, M. L. et al. Observation of current whirlpools in graphene at room temperature. Science 384, 465-469 (2024).
- 3. Sulpizio, J. A. et al. Visualizing Poiseuille flow of hydrodynamic electrons. Nature 576, 75-79 (2019).
- 4. Levitov, L. & Falkovich, G. Electron viscosity, current vortices and negative nonlocal resistance in graphene. *Nat. Phys.* **12**, 672–676 (2016).
- 5. Keser, A. C. et al. Geometric control of universal hydrodynamic flow in a two-dimensional electron fluid. *Phys. Rev. X* 11, 031030 (2021).
- 6. Moll, P. J., Kushwaha, P., Nandi, N., Schmidt, B. & Mackenzie, A. P. Evidence for hydrodynamic electron flow in PdCoO2. *Science* 351, 1061–1064 (2016).
- 7. Estrada-Álvarez, J., Domínguez-Adame, F. & Díaz, E. Anisotropic signatures of electron hydrodynamics. *Phys. Rev. Res.* 7, 013087 (2025)
- 8. Aharon-Steinberg, A. et al. Direct observation of vortices in an electron fluid. Nature 607, 74-80 (2022).
- 9. Varnavides, G., Yacoby, A., Felser, C. & Narang, P. Charge transport and hydrodynamics in materials. Nat. Rev. Mater. 8, 726 (2023).
- 10. Polini, M. & Geim, A. K. Viscous electron fluids. Phys. Today 73, 28-35 (2020).
- 11. Baker, G., Moravec, M. & Mackenzie, A. P. A perspective on non-local electronic transport in metals: viscous, ballistic, and beyond. *Ann. Phys.* **536**, 2400087 (2024).
- 12. Narozhny, B. N. Hydrodynamic approach to two-dimensional electron systems. Riv. Nuovo Cimento 45, 661 (2022).
- 13. Estrada-Álvarez, J. et al. Superballistic conduction in hydrodynamic antidot graphene superlattices. Phys. Rev. X 15, 011039 (2025).
- 14. Krishna-Kumar, R. et al. Superballistic flow of viscous electron fluid through graphene constrictions. *Nat. Phys.* **13**, 1182–1185 (2017).
- 15. Guo, H., Ilseven, E., Falkovich, G. & Levitov, L. S. Higher-than-ballistic conduction of viscous electron flows. PNAS USA 114, 3068–3073 (2017).
- 16. Gurzhi, R. N. Hydrodynamic effects in solids at low temperature. Sov. Phys. Uspekhi 11, 255 (1968).
- 17. Kravtsov, M. et al. Viscous terahertz photoconductivity of hydrodynamic electrons in graphene. Nat. Nanotech. 20, 51 (2024).
- 18. Estrada-Álvarez, J., Díaz García, E. & Dominguez-Adame, F. Negative differential resistance of viscous electron flow in graphene. 2D Mater. 12, 015012 (2024).
- 19. Stern, A. et al. How electron hydrodynamics can eliminate the Landauer-Sharvin resistance. *Phys. Rev. Lett.* **129**, 157701 (2022).
- 20. Huang, W., Paul, T., Perrin, M. L. & Calame, M. Eliminating the channel resistance in two-dimensional systems using viscous charge flow. 2D Mater. 11, 033001 (2024).
- 21. Estrada-Álvarez, J., Domínguez-Adame, F. & Díaz, E. Alternative routes to electron hydrodynamics. Commun. Phys. 7, 138 (2024).
- 22. Robinson, J. C. An Introduction to Ordinary Differential Equations (Cambridge University Press, 2004).
- 23. Kiselev, E. I. & Schmalian, J. Boundary conditions of viscous electron flow. Phys. Rev. B 99, 035430 (2019)
- 24. Ledwith, P. J., Guo, H. & Levitov, L. The hierarchy of excitation lifetimes in two-dimensional Fermi gases. *Ann. Phys.* 411, 167913 (2019).
- Ledwith, P., Guo, H., Shytov, A. & Levitov, L. Tomographic dynamics and scale-dependent viscosity in 2D electron systems. Phys. Rev. Lett. 123, 116601 (2019).
- 26. Hofmann, J. & Gran, U. Anomalously long lifetimes in two-dimensional Fermi liquids. Phys. Rev. B 108, L121401 (2023).
- 27. Hofmann, J. & Sarma, S. D. Collective modes in interacting two-dimensional tomographic fermi liquids. *Phys. Rev. B* **106**, 205412 (2022).
- 28. Alekseev, P. S. & Dmitriev, A. P. Viscosity of two-dimensional electrons. *Phys. Rev. B* **102**, 241409 (2020).
- 29. Rostami, H., Ben-Shachar, N., Moroz, S. & Hofmann, J. Magnetic field suppression of tomographic electron transport. *Phys. Rev.* B 111, 155434 (2025).
- 30. Estrada-Álvarez, J., Bermúdez-Mendoza, F., Domínguez-Adame, F. & Díaz, E. Optimal geometries for low-resistance viscous electron flow. *Phys. Rev. B* 111, 075401 (2025).
- 31. Zeng, Y. et al. Quantitative measurement of viscosity in two-dimensional electron fluids. arXiv preprint arXiv:2407.05026 (2024).
- 32. Alekseev, P. Negative magnetoresistance in viscous flow of two-dimensional electrons. Phys. Rev. Lett. 117, 166601 (2016).
- 33. Masubuchi, S. et al. Boundary scattering in ballistic graphene. Phys. Rev. Lett. 109, 036601 (2012).
- 34. Holder, T. et al. Ballistic and hydrodynamic magnetotransport in narrow channels. Phys. Rev. B 100, 245305 (2019).
- 35. Alekseev, P. S. & Semina, M. A. Ballistic flow of two-dimensional interacting electrons. Phys. Rev. B 98, 165412 (2018).
- 36. Alekseev, P. S. & Semina, M. A. Hall effect in a ballistic flow of two-dimensional interacting particles. *Phys. Rev. B* **100**, 125419 (2019).

- 37. Afanasiev, A., Alekseev, P., Greshnov, A. & Semina, M. Ballistic-hydrodynamic phase transition in flow of two-dimensional electrons. *Phys. Rev. B* **104**, 195415 (2021).
- 38. Nastasi, G. & Romano, V. Mathematical aspects and simulation of electron-electron scattering in graphene. Z. fur Angew. Math. Phys. 74, 28 (2023).
- Nazaryan, K. G. & Levitov, L. Nonlocal conductivity, continued fractions, and current vortices in electron fluids. Phys. Rev. B 110, 045147 (2024).
- 40. Kryhin, S., Hong, Q. & Levitov, L. Linear-in-temperature conductance in two-dimensional electron fluids. *Phys. Rev. B* 111, L081403 (2025).
- 41. Ben-Shachar, N. & Hofmann, J. Magnetotransport of tomographic electrons in a channel. arXiv preprint arXiv:2503.14431 (2025).
- 42. Ben-Shachar, N. et al. Near-hydrodynamic electron flow according to the linearized boltzmann equation. *Phys. Rev. B* 111, 125145 (2025).
- 43. Ben-Shachar, N. et al. Hall field and odd viscosity in near-hydrodynamic electron flows. Phys. Rev. B 111, L121107 (2025).
- 44. Alekseev, P. S. Viscous flow of two-component electron fluid in magnetic field. Semiconductors 57, 193-202 (2023).
- 45. Raichev, O. Linking boundary conditions for kinetic and hydrodynamic description of fermion gas. *Phys. Rev. B* **105**, L041301 (2022).
- 46. Raichev, O. Magnetohydrodynamic boundary conditions for the two-dimensional fermion gas. Phys. Rev. B 108, 125305 (2023).
- 47. Burnett, D. The distribution of molecular velocities and the mean motion in a non-uniform gas. *Prod. Lon. Math. Soc.* 2, 382–435 (1936).
- 48. Sendra, L. et al. Derivation of a hydrodynamic heat equation from the phonon boltzmann equation for general semiconductors. *Phys. Rev. B* **103**, L140301 (2021).
- 49. Soto, R. Kinetic Theory and Transport Phenomena, vol. 25 (Oxford University Press, 2016).
- 50. García-Colín, L. S., Velasco, R. M. & Uribe, F. J. Beyond the navier-stokes equations: burnett hydrodynamics. *Phys. Rep.* 465, 149–189 (2008).
- 51. Struchtrup, H. & Struchtrup, H. Macroscopic Transport Equations for Rarefied Gas Flows (Springer, 2005).
- 52. Struchtrup, H. & Taheri, P. Macroscopic transport models for rarefied gas flows: a brief review. IMA J. Appl. Math. 76, 672-697 (2011).
- 53. Jüngel, A. Transport equations for semiconductors, vol. 773 of Lecture Notes in Physics (Springer, 2009).
- Grasser, T., Tang, T.-W., Kosina, H. & Selberherr, S. A review of hydrodynamic and energy-transport models for semiconductor device simulation. *Proc. IEEE* 91, 251–274 (2003).
- 55. Hong, Q., Davydova, M., Ledwith, P. J. & Levitov, L. Superscreening by a retroreflected hole backflow in tomographic electron fluids. *Phys. Rev. B* **109**, 085126 (2024).
- $56. \ \ Ben-Shachar, N. \& \ Hofmann, J. \ Tomographic electron flow in confined geometries: Beyond the dual-relaxation time approximation. arXiv preprint arXiv:2503.14461 (2025).$
- 57. Alekseev, P. S. & Dmitriev, A. P. Hydrodynamic magnetotransport in two-dimensional electron systems with macroscopic obstacles. *Phys. Rev. B* **108**, 205413 (2023).
- 58. Dugaev, V. & Katsnelson, M. Edge scattering of electrons in graphene: Boltzmann equation approach to the transport in graphene nanoribbons and nanodisks. *Phys. Rev. B* 88, 235432 (2013).
- 59. Nastasi, G. et al. Direct simulation of charge transport in graphene nanoribbons. Commun. Comput. Phys. 31, 449-494 (2022).
- 60. Ciarlet, P. G. The Finite Element Method for Elliptic Problems (SIAM, 2002).

Acknowledgements

We wish to acknowledge R. Brito, R. Soto, and N. Ben-Shahar for discussions. This work was supported by the "(MAD2D-CM)-UCM" project funded by Comunidad de Madrid, by the Recovery, Transformation and Resilience Plan, and by NextGenerationEU from the European Union and Agencia Estatal de Investigación of Spain (Grants PID2019-106820RB-C2 and PID2022-136285NB-C31). J. E. acknowledges support from the Spanish Ministerio de Ciencia, Innovación y Universidades (Grant FPU22/01039).

Author contributions

J.E-A. Methodology, Investigation, Conceptualization, Writing-original draft. F.D-A. Investigation, Writing-review-editing, Funding acquisition. E.D. Investigation, Writing-review-editing, Funding acquisition, Supervision. All authors contributed to the final manuscript and approved it for publication.

Competing interests

The authors declare no competing interests.

Additional information

Supplementary Information The online version contains supplementary material available at https://doi.org/1 0.1038/s41598-025-22189-7.

Correspondence and requests for materials should be addressed to J.E.-Á.

Reprints and permissions information is available at www.nature.com/reprints.

Publisher's note Springer Nature remains neutral with regard to jurisdictional claims in published maps and institutional affiliations.

Open Access This article is licensed under a Creative Commons Attribution-NonCommercial-NoDerivatives 4.0 International License, which permits any non-commercial use, sharing, distribution and reproduction in any medium or format, as long as you give appropriate credit to the original author(s) and the source, provide a link to the Creative Commons licence, and indicate if you modified the licensed material. You do not have permission under this licence to share adapted material derived from this article or parts of it. The images or other third party material in this article are included in the article's Creative Commons licence, unless indicated otherwise in a credit line to the material. If material is not included in the article's Creative Commons licence and your intended use is not permitted by statutory regulation or exceeds the permitted use, you will need to obtain permission directly from the copyright holder. To view a copy of this licence, visit http://creativecommons.org/licenses/by-nc-nd/4.0/.

© The Author(s) 2025